

# The mechanism of nano-CuO and CuFe<sub>2</sub>O<sub>4</sub> catalyzed thermal decomposition of ammonium nitrate

Zhi-Xiang Xu<sup>1</sup>, Gui-Sheng Xu<sup>1</sup>, Xiao-Qi Fu<sup>2</sup>, and Qian Wang<sup>1</sup>

## Abstract

A new method was used to prepare nanocomposites (copper oxide, copper iron oxide). The copper oxide and copper iron oxide were characterized by powder X-ray diffraction, transmission electron microscope, and X-ray photoelectron spectra. Copper oxide/graphene oxide nanocatalyst was prepared during which copper oxide nanoparticle was simultaneously anchored on graphene oxide sheets. Copper iron oxide/graphene oxide was also prepared. In this work, the catalytic performance of the synthesized materials on the thermal decomposition of ammonium nitrate was investigated by thermogravimetric differential scanning calorimetry and thermogravimetric mass spectrometry. The results of thermogravimetric differential scanning calorimetry experiments indicated that nanocomposites catalyzed thermal decomposition of ammonium nitrate significantly, especially copper oxide/graphene oxide. The synergistic effect of copper iron oxide was not found. The activation energy of ammonium nitrate mixture was calculated respectively by Kissinger method. The initial temperature, peak temperature, and activation energy were significantly decreased. A new phenomenon, nitrous oxide formed at a very low temperature, was observed by mass spectra. Two stages of thermal decomposition phenomenon of ammonium nitrate catalyzed by copper oxide/graphene oxide were first observed according to thermogravimetric mass spectrometry results. The thermal decomposition mechanism of ammonium nitrate with copper oxide/graphene oxide was proposed according to thermogravimetric differential scanning calorimetry and thermogravimetric mass spectrometry results.

## Keywords

Ammonium nitrate, nano-oxide, graphene oxides, thermal decomposition

Date received: 27 July 2016; accepted: 6 November 2016

Topic: Nanoparticles

Topic Editor: Raphael Schneider

## Introduction

Ammonium perchlorate (AP) as the main oxidizer is using in most of the solid rocket propellants currently, but its products of combustion are toxic and not environmentally friendly. To overcome these environmental problems, it's necessary to investigate the use of the so-called clean burning propellants. Thus, many researchers are going to develop environmentally friendly oxidizers. Ammonium nitrate (AN) has attracted attention many years ago as a potential propellant oxidizer for no HCl presented in production of AN decomposition. However, poor ignitability,

hygroscopicity, low energy, low burning rate, and polymorphic transitions around room temperature limited the application of AN in solid rocket propellants.<sup>1–4</sup> Many

<sup>1</sup> School of Energy and Power Engineering, Jiangsu University, Zhenjiang, China

<sup>2</sup> School of Chemistry and Chemical Engineering, Jiangsu University, Zhenjiang, China

### Corresponding Author:

Zhi-Xiang Xu, School of Energy and Power Engineering, Jiangsu University, Zhenjiang 212013, China. Email: xuzx@ujs.edu.cn



researchers have attempted to overcome these problems to develop a wide range of practical applications for AN-based propellants. It's known that transition metal oxides (TMO) were effective additives to increase the burning rate and ignitability of AN propellants. Many researchers have reported that TMO was successfully used in AN-based propellant thermal decomposition.<sup>5–13</sup>

Graphene has attracted a great interest in both fundamental and applied areas.<sup>14,15</sup> It has excellent properties, especially huge surface area.<sup>16–18</sup> In recent years, many papers have reported graphene or graphene oxide (GO) to catalyze AP,<sup>19–24</sup> especially GO, which can easily absorb polar molecules to form different nanocomposites on carbon nanosheets.<sup>25,26</sup> However, a few literature has reported graphene- or GO-supported nanocomposites to catalyze AN. Therefore, it attracted great interests in developing GO-supported nanocomposites to catalyze AN thermal decomposition.

Ferric oxide ( $\text{Fe}_2\text{O}_3$ ) and copper oxide ( $\text{CuO}$ ) have been studied for excellent catalytic activity in solid propellants.<sup>27–31</sup> Copper iron oxide ( $\text{CuFe}_2\text{O}_4$ ) has also been reported in AP catalytic decomposition for its synergistic effect.<sup>32–34</sup> It has been reported that nano- $\text{CuO}$  and  $\text{Fe}_2\text{O}_3$  can catalyze decomposition in AN-based propellants.<sup>3,7,8,11–13</sup> However, no literature reported  $\text{CuFe}_2\text{O}_4$  composite oxides catalyzed AN thermal decomposition. For synergistic effect of composite oxides, thermal decomposition of AN can also be catalyzed by  $\text{CuFe}_2\text{O}_4$  composite oxides.

Since pure nanoparticles were likely to aggregate, the catalytic activity would be decreased notably. Therefore, a facile and reliable method was to anchor nanocomposites onto a supporter to prevent aggregation. Graphene/GO may be an ideal catalyst supporter. Based on this viewpoint, we expected that graphene/GO can dramatically improve the catalytic activity of nanoparticles as a catalyst supporter. Herein, we report a facile synthesis of  $\text{CuO}$  and  $\text{CuFe}_2\text{O}_4$  nanocomposites by an emulsion combustion method. Firstly, nanoparticles were characterized by powder X-ray diffraction (XRD), transmission electron microscope (TEM), and X-ray photoelectron spectra (XPS). The catalytic effect of  $\text{CuO}$ ,  $\text{CuO/GO}$ ,  $\text{CuFe}_2\text{O}_4$ , and  $\text{CuFe}_2\text{O}_4/\text{GO}$  nanocomposites on the thermal decomposition of AN was investigated by thermogravimetric differential scanning calorimetry (TG-DSC). Thermal decomposition kinetics of AN mixture were analyzed. The thermal decomposition mechanism was also analyzed by thermogravimetric mass spectrometry (TG-MS). The probable mechanism was also proposed.

## Experimental sections

### Materials

Copper nitrate ( $\text{Cu}(\text{NO}_3)_2 \cdot 3\text{H}_2\text{O}$ ; AR), ferric nitrate ( $\text{Fe}(\text{NO}_3)_3 \cdot 9\text{H}_2\text{O}$ ; AR), and ammonium nitrate (AN; AR) were used without further purification. Sorbitan monooleate

(SMO) and diesel were industrial materials. GO was self-made in laboratory from purified natural graphite (230 mesh, Qingdao Zhongtian Company, China) according to the method reported by Hummers and Offeman.<sup>35</sup>

### Synthesis and characterization of nanocatalyst

**Synthesis of  $\text{CuFe}_2\text{O}_4$  nanocatalyst by new method.** Nano- $\text{CuO}$  and  $\text{CuFe}_2\text{O}_4$  were synthesized by a new method. This process of synthesis of  $\text{CuO}$  and  $\text{CuFe}_2\text{O}_4$  nanoparticles was not reported in the previous study. It has two steps: (1) preparation of emulsion and (2) calcination of emulsion in furnace. The formation of emulsion was as follows:

Water ( $\text{H}_2\text{O}$ ):AN: $\text{Cu}(\text{NO}_3)_2 \cdot 3\text{H}_2\text{O}$ : $\text{Fe}(\text{NO}_3)_3 \cdot 9\text{H}_2\text{O}$ :  
SMO:diesel = 16:38:9.19:30.81:1.5:4.5

$\text{H}_2\text{O}$ :AN: $\text{Cu}(\text{NO}_3)_2 \cdot 3\text{H}_2\text{O}$ :SMO:diesel = 16:38:  
40:1.5:4.5

1. Preparation of emulsion: The procedure of emulsion prepared involved two steps. First, the oxidizer solution ( $\text{H}_2\text{O}$ , AN,  $\text{Cu}(\text{NO}_3)_2 \cdot 3\text{H}_2\text{O}$ , and  $\text{Fe}(\text{NO}_3)_3 \cdot 9\text{H}_2\text{O}$ ) was prepared by dissolving the ingredients in a large stainless steel beaker heated to a temperature of approximately  $80^\circ\text{C}$ . The oil phase (SMO and diesel) was then poured into the mixer bowl, when it was heated to  $60^\circ\text{C}$ , and maintained. Then, it was mixed with a speed of approximately 200 r/min, and the hot oxidizer solution was slowly poured into the bowl. After pouring, the speed of mixing was accelerated (approximately to 1200 r/min) and continued for a few seconds to achieve the final refinement.
2. Calcination of emulsion in furnace: The emulsion sample was then calcined in furnace at a temperature above  $600^\circ\text{C}$ . After heating for 2 h,  $\text{CuFe}_2\text{O}_4$  nanoparticles were collected. The solid was washed with ethanol and then used for further experiments. The nanoparticles were characterized by XRD and TEM. The preparation method of nano- $\text{CuO}$  was similar to that of  $\text{CuFe}_2\text{O}_4$ .

### Synthesis of $\text{CuFe}_2\text{O}_4/\text{GO}$ nanocatalyst and sample preparation.

The  $\text{CuFe}_2\text{O}_4/\text{GO}$  nanocomposite was synthesized in the following procedure. Hundred milligram of GO powder and 5 mL of n-butylamine were dispersed in 100 mL  $\text{H}_2\text{O}$  by sonication, forming stable GO colloid. After 1 h, a dispersion of 200 mg  $\text{CuFe}_2\text{O}_4$  was sonicated in 100 mL  $\text{H}_2\text{O}$ , and 5 mL ethylenediamine was added to the GO colloid solution. Subsequently, the mixture was heated to  $60^\circ\text{C}$  with magnetic stirring for 6 h. The bulk samples can be obtained by centrifugation of the mixture, and then washed with deionized  $\text{H}_2\text{O}$  and ethanol for several times. The  $\text{CuFe}_2\text{O}_4/\text{GO}$  nanocomposite was obtained after the precipitate was dried at  $60^\circ\text{C}$  under vacuum for 12 h. The preparation method of nano- $\text{CuO/GO}$  was similar to that of  $\text{CuFe}_2\text{O}_4/\text{GO}$ .

For the catalytic activity studies on CuO, CuFe<sub>2</sub>O<sub>4</sub>, CuO/GO, and CuFe<sub>2</sub>O<sub>4</sub>/GO, nanocatalyst was mixed with AN separately in a weight ratio 98:2 (wt%) by blending on a mechanical stirrer. The samples were named as follows:

- 1#: 2% CuO + 98% AN;
- 2#: 2% CuFe<sub>2</sub>O<sub>4</sub> + 98% AN;
- 3#: 2% CuO/GO + 98% AN; and
- 4#: 2% CuFe<sub>2</sub>O<sub>4</sub>/GO + 98% AN.

### XRD, TEM, and XPS analyses

The powder XRD analysis of the samples was carried out with a Bruker D8 (Bruker, Germany) SuperSpeed apparatus operating with a copper (Cu)  $K_\alpha$  radiation. The morphologies of the samples were investigated by JEM-2100 TEM (JEOL, Japan). XPS recorded on a Thermo ESCALAB250 (Thermo Fisher Scientific, USA) X-ray photoelectron spectrometer, using aluminum  $K_\alpha$  ( $h\nu = 1486.6$  eV). The binding energies were calibrated using C 1s peak of contaminant carbon (BE5284.6 eV) as an internal standard.

### Thermal decomposition of AN samples

Thermal decomposition experiments of AN samples were carried out under a nitrogen atmosphere with a NETZSCH STA449C (NETZSCH, Germany) instrument. In all experiments, 10 mg sample was loaded in a closed ceramic crucible with a pinhole in the cap and heated up from room temperature to 400°C. Nitrogen was used as a carrier gas with a flow rate of 20 mL/min. The heating rate was 2.5 K/min, 5 K/min, 10 K/min, and 20 K/min.

### TG-MS experiments

The TG-MS test was performed with NETZSCH STA449C system and MS (NETZSCHQMS403C, NETZSCH, Germany) system. NETZSCHQMS403C has the following conditions: ionizing electron energy of 70 eV, quartz capillary gas connector, and pressure injection 1000 mbar. Approximately 2 mg of sample was heated from 35°C to 400°C. The heating rate was 10 K/min, and the sample was carried in aluminum oxide crucibles. High-purity argon was used as purge gas with a gas flow rate of 20 mL/min.

### Decomposition kinetic analysis

The kinetics of the AN thermal decomposition with and without additive can be determined using the Kissinger method,<sup>36</sup> which uses the peak temperature ( $T_m$ ) at which the reaction rate is at a maximum as obtained from the DSC curves of samples decomposition in experiments with different heating rates. The equation was as follows

$$\ln\left(\frac{\beta}{T_m^2}\right) = \ln\left(\frac{AR}{E_a}\right) - \frac{E_a}{RT_m} \quad (1)$$

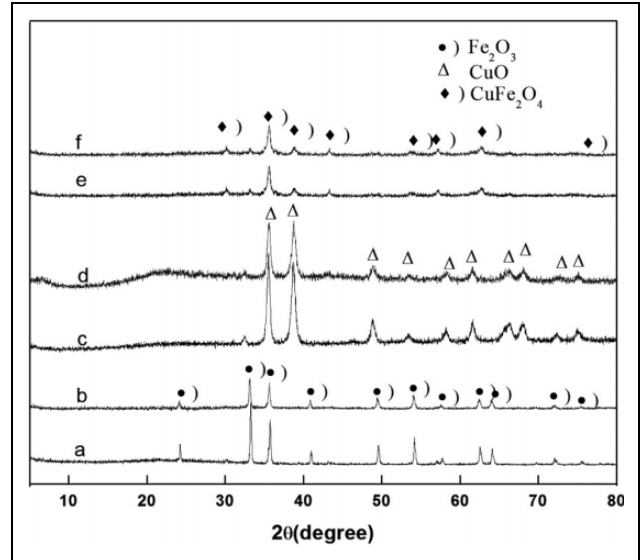


**Figure 1.** XRD of as-synthesized (a) Fe<sub>2</sub>O<sub>3</sub>, (b) Fe<sub>2</sub>O<sub>3</sub>/GO, (c) CuO, (d) CuO/GO, (e) CuFe<sub>2</sub>O<sub>4</sub>, and (f) CuFe<sub>2</sub>O<sub>4</sub>/GO composites. XRD: X-ray diffraction; Fe<sub>2</sub>O<sub>3</sub>: ferric oxide; GO: graphene oxide; CuO: copper oxide; CuFe<sub>2</sub>O<sub>4</sub>: copper iron oxide.

where  $\beta$  is the heating rate (K/min),  $T_m$  is the temperature,  $A$  is the pre-exponential factor,  $R$  is the gas constant, and  $E_a$  is the activation energy. The slope and intercept from the line plot of  $\ln(\beta/T_m^2)$  against  $1/T_m$  were used to obtain the activation energy and pre-exponential factor, respectively.

## Results and discussion

### Characteristic of nanocatalysts

The nanocatalysts were characterized by XRD, TEM, and XPS. The XRD results were listed in Figure 1. The diffraction peaks located in the range from 20° to 80° were all ascribed to the characteristic Bragg reflections of CuO (JCPDS 34-0394),  $\alpha$ -Fe<sub>2</sub>O<sub>3</sub> (JCPDS 33-0664), and CuFe<sub>2</sub>O<sub>4</sub> (JCPDS 30-1346), respectively. No obvious diffraction peaks of GO or graphene were observed. It indicated that CuO,  $\alpha$ -Fe<sub>2</sub>O<sub>3</sub>, and CuFe<sub>2</sub>O<sub>4</sub> particles were all attached to GO surface. Figure 2 showed the TEM images of as-synthesized CuO, CuFe<sub>2</sub>O<sub>4</sub>, CuO/GO, and CuFe<sub>2</sub>O<sub>4</sub>/GO. The results found a slight aggregation of metal oxide particles (CuO and CuFe<sub>2</sub>O<sub>4</sub>). The average sizes of CuO and CuFe<sub>2</sub>O<sub>4</sub> were 83 and 13 nm, respectively. The GO prevented the aggregation of metal oxide particles, and most CuO and CuFe<sub>2</sub>O<sub>4</sub> nanoparticles distributed randomly on GO sheets.

To explore Cu and iron (Fe) elements on the surface of CuFe<sub>2</sub>O<sub>4</sub> composites, XPS spectra were measured. Figure 3 depicted the Cu 2p and Fe 2p XPS spectra of different samples. The Cu 2p spectrum of CuO and CuFe<sub>2</sub>O<sub>4</sub> samples showed the typical structure. The Cu 2p signal was composed of peak at 933 eV. The result was assigned to the presence of CuO species. The Cu 2p<sub>3/2</sub> and Cu 2p<sub>1/2</sub> peaks were accompanied by distinct shake-up at about binding energies of 944 eV and 963 eV, which were the

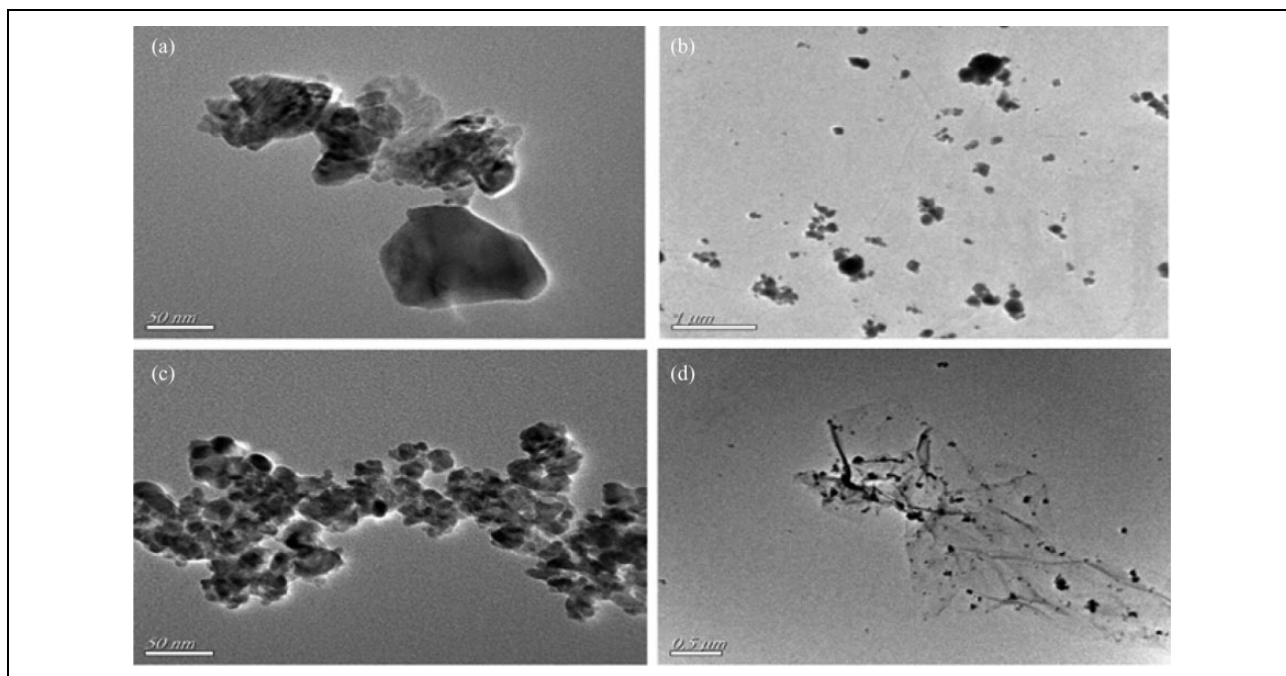


**Figure 2.** TEM images of (a) CuO, (b) CuO/GO, (c) CuFe<sub>2</sub>O<sub>4</sub> and (d) CuFe<sub>2</sub>O<sub>4</sub>/GO composites. TEM: transmission electron microscope; CuO: copper oxide; GO: graphene oxide; CuFe<sub>2</sub>O<sub>4</sub>: copper iron oxide.

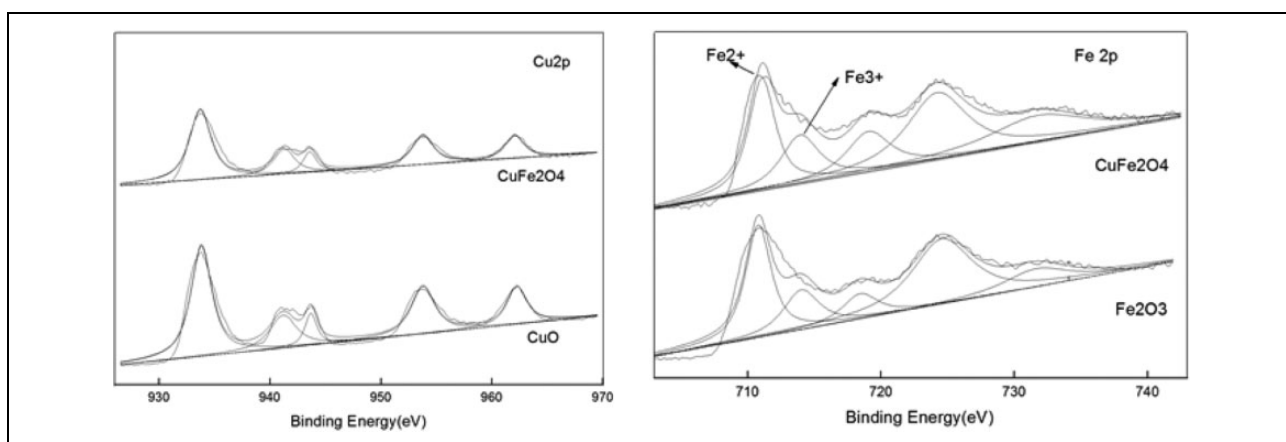


**Figure 3.** (a) Cu 2p XPS spectra of samples; (b) Fe 2p XPS spectra of samples. Cu: copper; XPS: X-ray photoelectron spectra; Fe: iron.

characteristic of Cu<sup>2+</sup>. The results testified that a part of Cu species were incorporated into the framework in the form of CuFe<sub>2</sub>O<sub>4</sub>. Comparing CuO with CuFe<sub>2</sub>O<sub>4</sub> XPS spectra, we can confirm the Cu species was on the external surface of CuFe<sub>2</sub>O<sub>4</sub> catalysts. The XPS spectra of Fe 2p of CuFe<sub>2</sub>O<sub>4</sub> catalysts were showed in Figure 3(b). For Fe 2p XPS spectra, each peak can be split. One of the Fe 2p<sub>3/2</sub> doublet peaks was at 710.8 eV and the second one was at 713.8 eV. Hence, from XPS results, the peak of Cu2p and Fe2p almost has no change. From XPS results, we can also confirm the Fe species was on the external surface of CuFe<sub>2</sub>O<sub>4</sub> catalysts. The species ratio of Cu:Fe = 16.62:33.1. The result was the same with mole ratio of CuFe<sub>2</sub>O<sub>4</sub>. The XPS results showed that ferric and Cu species were distributed well proportionally on the surface of CuFe<sub>2</sub>O<sub>4</sub> sample.

### *The influence on the thermal decomposition of AN with catalysts*

The CuO, CuFe<sub>2</sub>O<sub>4</sub>, CuFe<sub>2</sub>O<sub>4</sub>/GO, or CuO/GO composite was explored as a catalyst to the thermal decomposition of AN, respectively. The reference has found that GO has little influence on thermal decomposition of AP even at high temperature (>350°C).<sup>20,21</sup> Hence, GO was not investigated to catalyze thermal decomposition of AN again for AN decomposition temperature lower than 350°C. The performances of CuO, CuFe<sub>2</sub>O<sub>4</sub>, CuFe<sub>2</sub>O<sub>4</sub>/GO, and CuO/GO composite on the thermal decomposition of AN were investigated by TG-DSC. The results were showed in Figure 4. The DSC curve of Figure 4(a) revealed that prior to 170°C, appeared endothermic peak was phase transition of AN;

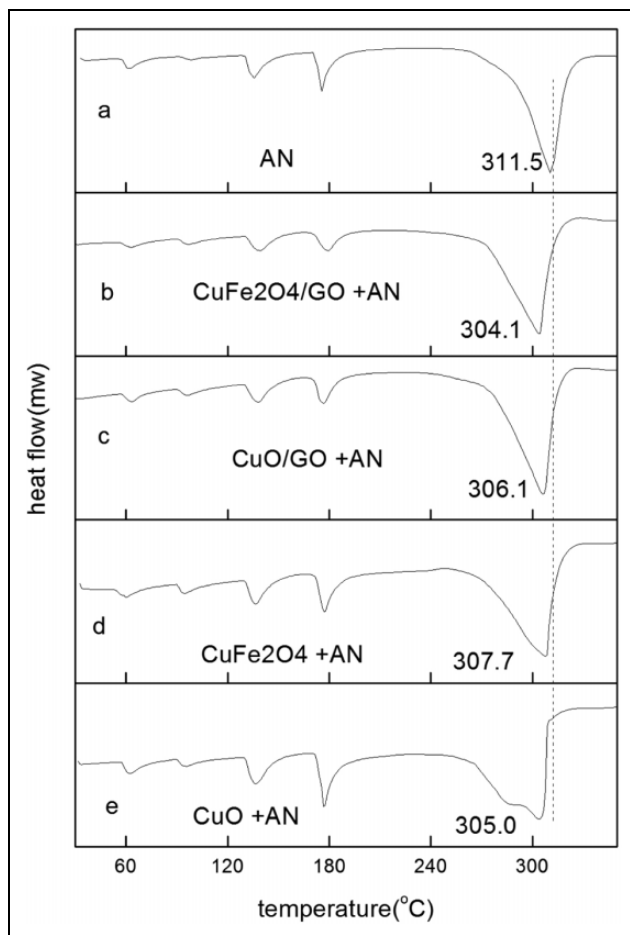


**Figure 4.** DSC curves for: (a) pure AN, (b) AN + CuFe<sub>2</sub>O<sub>4</sub>/GO, (c) AN + CuO/GO, (d) AN + CuFe<sub>2</sub>O<sub>4</sub>, and (e) AN + CuO at a heating rate of 10 K/min. DSC: differential scanning calorimetry; AN: ammonium nitrate; CuFe<sub>2</sub>O<sub>4</sub>: copper iron oxide; GO: graphene oxide; CuO: copper oxide.

after 170°C, thermal decomposition of AN was carried out. The other samples also have the same tendency. As can be seen from Figure 4, it's shown that, compared with pure AN, decomposition temperature of AN mixture with 2% CuO and CuO/GO shifted to a low temperature notably. Aforementioned papers found that synergistic effect of CuFe<sub>2</sub>O<sub>4</sub> presented in catalyzed AP.<sup>32–34</sup> However, the present article found no synergistic effect of CuFe<sub>2</sub>O<sub>4</sub>. The reference found that Cu-based catalysts have been found to be highly active at relatively low temperatures (<350°C). But Fe-based catalysts were at high temperatures (>300°C).<sup>37</sup> For thermal decomposition temperature of AN about 300°C at the present experimental condition, the Cu activity was stronger than Fe. The XPS results showed that Fe<sub>2</sub>O<sub>3</sub> distributed on the surface of CuFe<sub>2</sub>O<sub>4</sub> sample was well proportioned. Therefore, we can explain the synergistic effect of CuFe<sub>2</sub>O<sub>4</sub> was not found in AN mixture thermal decomposition process.

When GO was added as a catalyst supporter, decomposition temperature of AN with CuO/GO shifted to a low

**Table 1.** Thermal properties of AN with additives.<sup>a</sup>

Samples	$T_i$ (°C)	$T_p$ (°C)	$E$	$\ln A$	$R^2$
AN + CuO	238.7220	305.0	115.0172	23.1159	0.98194
AN + CuFe <sub>2</sub> O <sub>4</sub>	244.9395	307.7	121.3096	24.3741	0.98052
AN + CuO/GO	235.5852	306.1	75.7915	14.4976	0.89875
AN + CuFe <sub>2</sub> O <sub>4</sub> /GO	240.9537	304.1	106.4146	21.2467	0.99285
Pure AN	247.3800	311.5	162.7335	58.4185	0.99859

AN: ammonium nitrate; CuO: copper oxide; CuFe<sub>2</sub>O<sub>4</sub>: copper iron oxide; GO: graphene oxide;  $T_i$ : initial decomposition temperature;  $T_p$ : peak temperature;  $E$ : activation energy;  $\ln A$ : pre-exponential factor;  $R^2$ : correlation coefficient.

<sup>a</sup> $T_i$  and  $T_p$  were valued at a heating rate of 10 K/min.  $T_i$  was temperature at the 5% mass loss according to Li et al.<sup>38</sup>

temperature about 5°C. It means the catalytic activity of catalytic agent increased. However, to our surprise, the peak temperature of AN with CuFe<sub>2</sub>O<sub>4</sub>/GO shifted to a low temperature about 7°C. It must combine with activation energy to confirm catalysis results.

In order to analyze the catalysis of CuO, CuFe<sub>2</sub>O<sub>4</sub>, CuO/GO, or CuFe<sub>2</sub>O<sub>4</sub>/GO to AN thermal decomposition, the activation energy and initial decomposition temperature were listed in Table 1. From Table 1, the initial temperature and peak temperature significantly decreased when CuO/GO was added to AN, and also CuFe<sub>2</sub>O<sub>4</sub>/GO has excellent catalysis but catalytic activity was lower than CuO/GO. We also have found the activation energy required for the thermal decomposition of pure AN to be 162.7335 kJ/mol. Although the reported activation energy for pure AN decomposition varies from 86.2 kJ/mol to 206.9 kJ/mol, previous researchers in this area agreed that the overall decomposition reaction of AN was described by the first-order reaction kinetics.<sup>39</sup> The activation energy of AN mixture decreased notably, especially in 3#. In other words, the reaction kinetics process of AN with additives perhaps was changed. The reaction kinetics process was not first-order reaction kinetics. Hence, according to initial temperature, peak temperature, and activation energy, we can obtain that additives catalyzed AN thermal decomposition significantly, especially CuO/GO. The difference of CuO/GO and CuFe<sub>2</sub>O<sub>4</sub>/GO was also observed. The activation energy of CuFe<sub>2</sub>O<sub>4</sub> with and without GO almost has no discrepancy. But CuO was very notable. The reason perhaps was that Fe<sub>2</sub>O<sub>3</sub> has little effect on AN thermal decomposition.<sup>8</sup> Hence, the effective content of catalytic activity materials of CuFe<sub>2</sub>O<sub>4</sub>/GO was fewer than CuO/GO. In other words, CuO/GO has more remarkable catalytic activity than CuFe<sub>2</sub>O<sub>4</sub>/GO to AN thermal decomposition.

In the experiment process, we also found the sample mass notably effected the AN thermal decomposition. The results were listed in Online Supplementary Figure S1. Li et al.<sup>38</sup> also found the same results. Koga found that the activation energy of AN decomposition decreased slightly with increasing sample mass in the range of 5–15 mg using TG.<sup>40,41</sup> Hence, we selected less mass sample to analyze TG-MS in the next TG-MS experiments.

### Evolved gas analysis

In order to analyze the decomposition mechanism of AN with additives, samples were chosen to perform the evolved gas analysis. Real-time mass spectral analysis of the evolved gases was also performed. The DSC curves of samples were listed in Online Supplementary Figure S2. The MS results of the evolved gases were listed in Online Supplementary Figures S3 to S6. It showed the ion current curves for mass-to-charge ( $m/z$ ) ratios = 16, 17, 18, 30, 44, 46, 63. The peaks were assigned to ammonia ( $\text{NH}_3$ ;  $m/z$  = 16, 17),  $\text{H}_2\text{O}$  ( $m/z$  = 17, 18), nitric oxide ( $\text{NO}$ ;  $m/z$  = 30), nitrous oxide ( $\text{N}_2\text{O}$ ;  $m/z$  = 44), nitric acid ( $\text{HNO}_3$ ;  $m/z$  = 30, 46, 63), and nitrogen dioxide ( $\text{NO}_2$ ;  $m/z$  = 46).

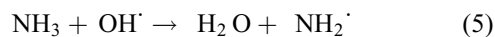
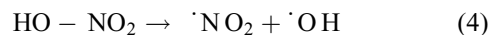
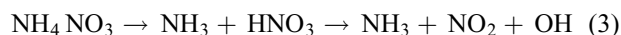
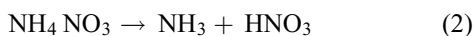
For dissociation reaction of AN presented even at low temperature,<sup>42</sup> the species ( $m/z$  = 17) at low temperature appeared, and it was ascribed to  $\text{NH}_3$ . From Online Supplementary Figures S3 to S6, the curve change showed the presence of  $\text{NH}_3$ . Then,  $\text{NH}_3$  can further undergo pyrolysis but needs high temperature. The  $\text{HNO}_3$  (g) ( $m/z$  = 63) was also detected, and it can demonstrate dissociation reaction of AN presented at very low temperature. The  $\text{NH}_3$  was found at 130°C in isothermal experiments.<sup>43</sup> Liu<sup>44</sup> also detected species ( $m/z$  = 15, 16,  $\cdot\text{NH}$ ,  $\cdot\text{NH}_2$ ) at low temperature (100°C). However, Liu thought it presented at very high temperature.<sup>45,46</sup> During the reaction process,  $\text{NO}_2$  ( $m/z$  = 46) was also detected. The species ( $m/z$  = 44) was  $\text{N}_2\text{O}$  not  $\text{CO}_2$  at present experimental condition.

Based on above analysis of the results from the present study, the thermal decomposition of AN with additives has been changed. And it needed to further analyze in the next paragraph.

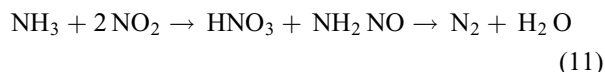
### Catalytic mechanism of the thermal decomposition of AN catalyzed by nanocomposites

Thermal decomposition of AN has been researched widely.<sup>1–4</sup> Many researchers have been proposed thermal decomposition mechanism. Oxley proposed a widely accepted mechanism. Oxley<sup>47,48</sup> showed that the decomposition mechanism of AN followed two pathways: an ionic reaction and a radical reaction. The ionic reaction occurred at low temperature and has relatively low speed. The radical reaction occurred at high temperature.

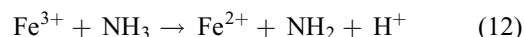
AN melted at 169°C and began to decompose as soon as it melted. Reaction (2) was generally accepted as the thermal decomposition initiating reaction, which was an endothermic proton transfer. However, Izato and Miyake found that the molten AN was first dissociated to  $\text{NH}_4^+$  and  $\text{NO}_3^-$ . The  $\text{NO}_3^-$  in molten AN was more stable than the  $\text{HNO}_3$ .<sup>49</sup> When the molten AN was heated from 470 K to 500 K, exothermic decomposition reaction (3) occurred.<sup>50</sup> Reaction (3) was more common and was the basis of commercial production of  $\text{N}_2\text{O}$ .



However, since the activation energy of the homolysis of  $\text{HNO}_3$  was very high at about 190 kJ/mol, it was the rate-controlling step. Hence, at high temperature, the ionic mechanism of AN decomposition was overtaken by radical reactions,<sup>51</sup> with homolysis of  $\text{HNO}_3$  being the rate-controlling step<sup>3</sup> as shown in reaction (4). The MS also detected  $\text{NO}_2$ . The reference also found the energy barrier was lowest in different reaction pathways.<sup>52</sup> Then amidogen radical ( $\text{NH}_2 \cdot$ ) was reacted as showed in reactions (5) and (6). But Cagnina et al.<sup>53</sup> thought  $\text{NH} \cdot$  was formed as showed in reaction (7). It was further reacted as showed in reactions (8)–(10). Hence, we thought  $\text{NO}_2 \cdot$  was easy to be formed at high temperature. When heated above 500 K, reaction (3) was the dominant decomposition pathway. On the basis of reaction (11), the following mechanism has been reported<sup>3,47,54–56</sup>



$\text{Fe}_2\text{O}_3$  has showed excellent catalysis in  $\text{NH}_3$ -Selective Catalytic Reduction (SCR). It was widely accepted that it can interact with  $\text{NH}_3$ .<sup>57</sup> The reaction was as follows (reaction (12))



$\text{CuO}$  has also been found to have same reaction. When  $\text{NH}_3$  was absorbed on the nanoparticle surface, the reaction carried out by the formation of  $\text{CuO}$  and  $\text{NH}_3$  and amine ( $\text{NH}_2$ ).<sup>58</sup> However, Vargeese and Muralidharan proposed new viewpoint.<sup>59</sup> There was no  $\text{NH}_2$  formed during the reaction process. If  $\text{NH}_2$  formed, the curve of ion current would change. The results of ion current curve of  $\text{NH}_2$  were listed in Figure 5. The discrepancy of different samples was little except  $\text{CuO/GO}$ . At about 190°C, the ion current notably changed, which means  $\text{NH}_2$  formed. It can be oxidized easily by oxidizing gas. To our surprise, ion current

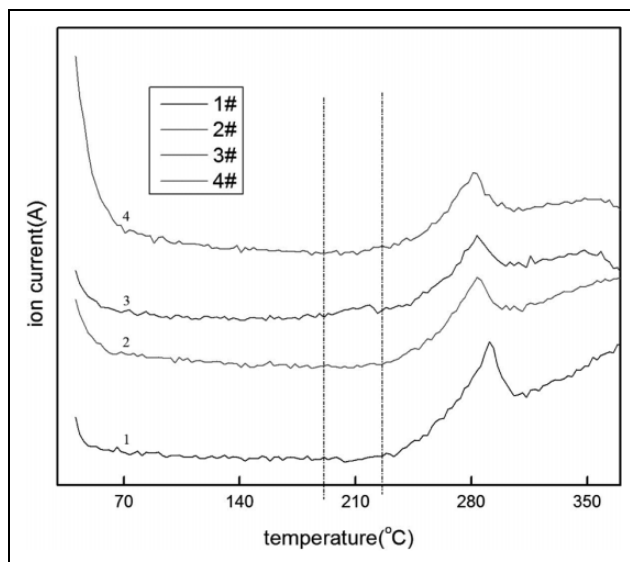


**Figure 5.** Ion current curve of  $\text{NH}_2$  ( $m/z = 16$ ).  $\text{NH}_2$ : amine;  $m/z$ : mass-to-charge ratio.

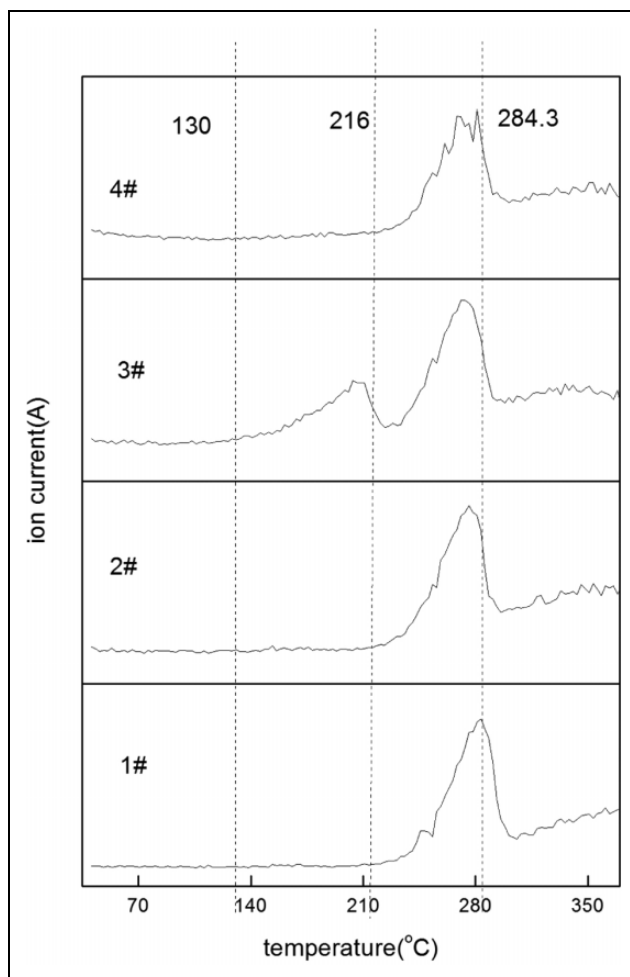


**Figure 6.** Ion current curve of  $\text{N}_2\text{O}$  ( $m/z = 44$ ).  $\text{N}_2\text{O}$ : nitrous oxide;  $m/z$ : mass-to-charge ratio.

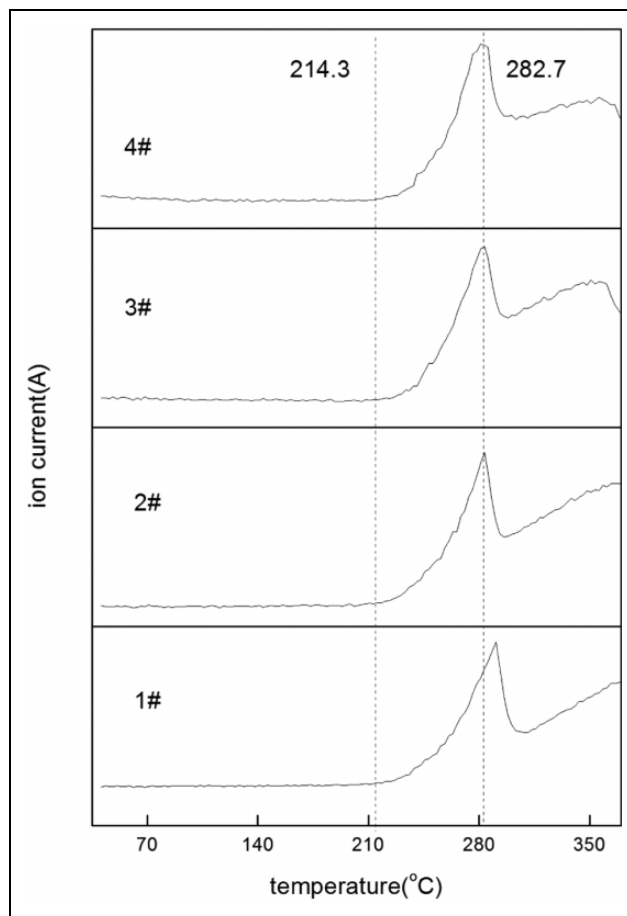
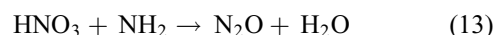


**Figure 7.** Ion current curve of  $\text{NO}$  ( $m/z = 30$ ).  $\text{NO}$ : nitric oxide;  $m/z$ : mass-to-charge ratio.

curve of  $\text{N}_2\text{O}$  was very strange. From Figure 6, we can find that  $\text{N}_2\text{O}$  formed at very low temperature of 3# at about  $130^\circ\text{C}$ . Chen et al.<sup>60</sup> thought  $\text{N}_2\text{O}$  was formed when  $\text{NH}_3$  reacted with  $\text{NO}_x$  at less than  $200^\circ\text{C}$ . According to Andersen et al.'s<sup>50</sup> results, the  $\text{NO}_2$  must be presented to form  $\text{N}_2\text{O}$ . However, at present condition,  $\text{NO}_2$  was very difficult to form below  $200^\circ\text{C}$  or little amount. Oxidizing gas was just only  $\text{HNO}_3$ , it can also be found at very low temperature.<sup>42</sup> Another oxidizing species was  $\text{NO}_3^-$  according to Izato and Miyake.<sup>49</sup> That is to say, it presented a new thermal decomposition pathway. The possible mechanism of thermal decomposition was  $\text{HNO}_3/\text{NO}_3^-$ -oxidized  $\text{NH}_2$  directly. The reactivity of  $\text{HNO}_3$  is stronger than  $\text{NO}_3^-$ . In this condition,  $\text{HNO}_3$  perhaps played an important role. Wang et al.<sup>43</sup> and Xu et al.<sup>61</sup> also found  $\text{HNO}_3$  can oxidize low-molecular-weight materials. According to these results, the reaction to form  $\text{N}_2\text{O}$  was proposed as follows:



However, from Figure 6, we also found that  $\text{N}_2\text{O}$  was formed in two stages. When temperature was heated to more than  $200^\circ\text{C}$ , the  $\text{NO}_x$  was detected. It means  $\text{NH}_2$  can be oxidized by  $\text{NO}_x$ . Hence, the two stages of  $\text{N}_2\text{O}$  mean

the mechanism of AN thermal decomposition was changed. The mechanism of AN thermal decomposition was proposed. At low temperature ( $<200^{\circ}\text{C}$ ), most likely mechanism was that  $\text{NH}_2$  was oxidized by  $\text{HNO}_3$  or  $\text{NO}_3^-$  to form  $\text{N}_2\text{O}$ , especially  $\text{HNO}_3$ . In the process,  $\text{CuO}$  played an important role.  $\text{CuO}$  absorbed  $\text{NH}_3$  to form  $\text{NH}_2$ . This process promoted AN disassociation reaction to form large amount of  $\text{HNO}_3$ . As we all know, acid catalyzed AN thermal decomposition.<sup>54</sup> Hence,  $\text{CuO}$  can catalyze AN thermal decomposition notably, especially  $\text{CuO}/\text{GO}$ . The fundamental reason was that  $\text{HNO}_3$  catalyzed AN thermal decomposition at low temperature.

Zhang et al. thought  $\text{NO}$  played an important role in the  $\text{NO}_x$  and  $\text{NH}_3$  catalytic reaction by  $\text{CuO}$ .<sup>37</sup> However, Figure 7 showed no change in the ion current of  $\text{NO}$ . Hence, in the present research, the mechanism of AN thermal decomposition might be different from the results of Zhang et al.<sup>37</sup> and Janssens et al.<sup>59</sup>

## Conclusion

In summary,  $\text{CuO}/\text{GO}$  and  $\text{CuFe}_2\text{O}_4/\text{GO}$  nanocomposites were successfully obtained by a new emulsion combustion method and they showed an intensive catalytic effect on the thermal decomposition of AN. The catalytic agent was characterized by XRD, TEM, and XPS. The initial temperature, peak temperature, and activation energy were notably decreased when  $\text{CuO}/\text{GO}$  was added to AN.  $\text{Fe}_2\text{O}_3$  distributed on the surface of  $\text{CuFe}_2\text{O}_4$ , and  $\text{Fe}_2\text{O}_3$  has little effect on AN thermal decomposition. Therefore, the synergistic effect was not found when  $\text{CuFe}_2\text{O}_4/\text{GO}$  was added to AN. An important phenomenon was that  $\text{N}_2\text{O}$  was formed at very low temperature around  $140^{\circ}\text{C}$  during the AN thermal decomposition process. We considered that it was formed by  $\text{HNO}_3$  and  $\text{NH}_2$  reaction at low temperature. The mechanism of thermal decomposition of AN with  $\text{CuO}/\text{GO}$  was proposed. The formed intermediate of  $\text{NH}_2$  was found to be a very important factor to progress the catalytic reaction of AN decomposition.

## Declaration of conflicting interests

The author(s) declared no potential conflicts of interest with respect to the research, authorship, and/or publication of this article.

## Funding

The author(s) disclosed receipt of the following financial support for the research, authorship, and/or publication of this article: The article was supported by Inner Mongolia Sheng An Chemical Ltd Co. and the Foundation of Jiangsu University of Advanced scholars (15JDG159), Natural Science Foundation of Jiangsu Colleges and Universities (16KJB150010).

## Supplemental material

The online data supplements are available at <http://journals.sagepub.com/doi/suppl/10.1177/1847980416681699>.

## References

1. Oommen C and Jain SR. Ammonium nitrate: a promising rocket propellant oxidizer. *J Hazard Mater* 1999; 67: 253–281.
2. Shalini C and Dave PN. Review on thermal decomposition of ammonium nitrate. *J Energ Mater* 2013; 31: 1–26.
3. Sinditskii V, Egorshv V, Levshenkov A, et al. Ammonium nitrate: combustion mechanism and the role of additives. *Propell Explos Pyrotech* 2005; 30: 269–280.
4. Singh G and Prem SF. Studies on energetic compounds: Part 36: evaluation of transition metal salts of NTO as burning rate modifiers for HTPB-AN composite solid propellants. *Combust Flame* 2003; 135: 145–150.
5. Naya T and Kohga M. Burning characteristics of ammonium nitrate-based composite propellants supplemented with  $\text{MnO}_2$ . *Propell Explos Pyrotech* 2013; 38: 87–94.
6. Chandru RA, Patra S, Oommen C, et al. Exceptional activity of mesoporous  $\beta\text{-MnO}_2$  in the catalytic thermal sensitization of ammonium perchlorate. *J Mater Chem* 2012; 22: 6536–6538.
7. Kohga M and Naya T. Thermal decomposition behaviors and burning characteristics of AN/RDX-based composite propellants supplemented with  $\text{MnO}_2$  and  $\text{Fe}_2\text{O}_3$ . *J Energ Mater* 2015; 33: 288–304.
8. Naya T and Kohga M. Burning characteristics of ammonium nitrate-based composite propellants supplemented with  $\text{Fe}_2\text{O}_3$ . *Propell Explos Pyrotech* 2013; 38: 547–554.
9. Vargeese AA and Muralidharan K. Anatase–brookite mixed phase nano  $\text{TiO}_2$  catalyzed homolytic decomposition of ammonium nitrate. *J Hazard Mater* 2011; 192: 1314–1320.
10. Vargeese AA, Muralidharan K, and Krishnamurthy VN. Kinetics of nano titanium dioxide catalyzed thermal decomposition of ammonium nitrate and ammonium nitrate-based composite solid propellant. *Propell Explos Pyrotech* 2015; 40: 260–266.
11. Kajiyama K, Izato Y, and Miyake A. Thermal characteristics of ammonium nitrate, carbon, and copper (II) oxide mixtures. *J Therm Anal Calorim* 2013; 113: 1475–1480.
12. Naya T and Kohga M. Influence of  $\text{Fe}_2\text{O}_3$  size on burning characteristics of ammonium nitrate/ $\text{Fe}_2\text{O}_3$  propellants. *J Propul Power* 2014; 30: 864–866.
13. Izato Y and Miyake A. Combustion characteristics of ammonium nitrate and carbon mixtures based on a thermal decomposition mechanism. *Propell Explos Pyrotech* 2013; 38: 129–135.
14. Pumera M and Wong CHA. Graphene and hydrogenated graphene. *Chem Soc Rev* 2013; 42: 5955–5987.
15. Wu Z, Ren W, Wen L, et al. Graphene anchored with  $\text{Co}_3\text{O}_4$  nanoparticles as anode of lithium ion batteries with enhanced reversible capacity and cyclic performance. *ACS Nano* 2010; 4: 3187–3194.
16. Zhu Y, Murali S, Cai W, et al. Graphene and graphene oxide: synthesis, properties, and applications. *Adv Mater* 2010; 22: 3906–3924.



17. Miller JR, Outlaw R, and Holloway B. Graphene double-layer capacitor with ac line-filtering performance. *Science* 2010; 329: 1637–1639.
18. Li X, Cai W, An J, et al. Large-area synthesis of high-quality and uniform graphene films on copper foils. *Science* 2009; 324: 1312–1314.
19. Li N, Geng Zh, Cao M, et al. Well-dispersed ultrafine  $\text{Mn}_3\text{O}_4$  nanoparticles on graphene as a promising catalyst for the thermal decomposition of ammonium perchlorate. *Carbon* 2013; 54: 124–132.
20. Xu C, Wang X, Zhu J, et al. Deposition of  $\text{Co}_3\text{O}_4$  nanoparticles onto exfoliated graphite oxide sheets. *J Mater Chem* 2008; 18: 5625–5629.
21. Yuan Y, Jiang W, Wang Y, et al. Hydrothermal preparation of  $\text{Fe}_2\text{O}_3$ /graphene nanocomposite and its enhanced catalytic activity on the thermal decomposition of ammonium perchlorate. *Appl Surf Sci* 2014; 303: 354–359.
22. Abhijit D, Javaid A, Pankaj V, et al. Graphene-iron oxide nanocomposite (GINC): an efficient catalyst for ammonium perchlorate (AP) decomposition and burn rate enhancer for AP based composite propellant. *RSC Adv* 2015; 5: 1950–1960.
23. Lan Y, Jin M, and Luo Y. Preparation and characterization of graphene aerogel/ $\text{Fe}_2\text{O}_3$ /ammonium perchlorate nano-structured energetic composite. *J Sol-Gel Sci Tech* 2015; 74: 161–167.
24. Li N, Cao M, Wu Q, et al. A facile one-step method to produce Ni/graphene nanocomposites and their application to the thermal decomposition of ammonium perchlorate. *CrystEngComm* 2012; 14: 428–434.
25. Cai D and Song M. Preparation of fully exfoliated graphite oxide nanoplatelets inorganic solvents. *J Mater Chem* 2007; 17: 3678–3680.
26. McAllister MJ, Li J, Adamson DH, et al. Single sheet functionalized graphene by oxidation and thermal expansion of graphite. *Chem Mater* 2007; 19: 4396–4404.
27. Patil PR, Krishnamurthy VN, and Joshi SS. Effect of nano-copper oxide and copper chromite on the thermal decomposition of ammonium perchlorate. *Propell Explos Pyrotech* 2008; 33: 266–270.
28. Sharma JK, Srivastava P, Singh G, et al. Catalytic thermal decomposition of ammonium perchlorate and combustion of composite solid propellants over green synthesized  $\text{CuO}$  nanoparticles. *Thermoch Acta* 2015; 614: 110–115.
29. Patil PR, Krishnamurthy VN, and Joshi SS. Differential scanning calorimetric study of HTPB based composite propellants in presence of nano ferric oxide. *Propell Explos Pyrotech* 2006; 31: 442–446.
30. Vargeese AA, Mija SJ, and Muralidharan K. Effect of copper oxide, titanium dioxide, and lithium fluoride on the thermal behavior and decomposition kinetics of ammonium nitrate. *J Energ Mater* 2014; 32: 146–161.
31. Gurdip S, Inder Pal SK, and Shalini D. Kinetics of thermal decomposition of ammonium perchlorate with nanocrystals of binary transition metal ferrites. *Propell Explos Pyrotech* 2009; 34: 72–77.
32. Liu T, Wang L, Yang P, et al. Preparation of nanometer  $\text{CuFe}_2\text{O}_4$  by auto-combustion and its catalytic activity on the thermal decomposition of ammonium perchlorate. *Mater Lett* 2008; 62: 4056–4058.
33. Wang Y, Xia X, Zhu J, et al. Catalytic activity of nanometer-sized  $\text{CuO}/\text{Fe}_2\text{O}_3$  on thermal decomposition of AP and combustion of AP-based propellant. *Combust Sci Tech* 2011; 183: 154–162.
34. Liu H, Jiao Q, Zhao Y, et al. Cu/Fe hydrotalcite derived mixed oxides as new catalyst for thermal decomposition of ammonium perchlorate. *Mater Lett* 2010; 64: 1698–1700.
35. Hummers WS and Offeman RE. Preparation of graphitic oxide. *J Am Chem Soc* 1958; 80: 1339–1339.
36. Kissinger HE. Reaction kinetics in differential thermal analysis. *Anal Chem* 1957; 29: 1702–1706.
37. Zhang T, Li J, Liu J, et al. High activity and wide temperature window of Fe-Cu-SSZ-13 in the selective catalytic reduction of NO with ammonia. *AIChE J* 2015; 61: 3825–3837.
38. Li X, Liu X, Cheng Y, et al. Thermal decomposition properties of double-base propellant and ammonium perchlorate. *J Therm Anal Calorim* 2014; 115: 887–894.
39. Gunawan R and Zhang D. Thermal stability and kinetics of decomposition of ammonium nitrate in the presence of pyrite. *J Hazard Mater* 2009; 165: 751–758.
40. Koga N and Tanaka H. Effect of sample mass on the kinetics of thermal decomposition of a solid. Part 3. Non-isothermal mass loss process of molten  $\text{NH}_4\text{NO}_3$ . *Thermochim Acta* 1994; 240: 141–151.
41. Koga N and Tanaka H. Effect of sample mass on the kinetics of thermal decomposition of a solid. Part 1. Isothermal mass-loss process of molten  $\text{NH}_4\text{NO}_3$ . *Thermochim Acta* 1992; 209: 127–134.
42. Östmark H, Wallin S, and Ang HG. Vapor pressure of explosives: a critical review. *Propell Explos Pyrot* 2012; 37: 12–23.
43. Wang S, Xu Z, and Wang Q. Thermal decomposition mechanism of emulsion explosives with phosphatide. *J Therm Anal Calorim* 2016; 124: 1053–1062.
44. Liu Z. *Thermal analyses for energetic materials*. Beijing: National Defense Industry Press, 2008.
45. Patil DG, Jain SR, and Brill TB. Thermal decomposition of energetic materials 56, on the fast thermolysis mechanism of ammonium nitrate and its mixtures with magnesium and carbon. *Propell Explos Pyrot* 1992; 17: 99–105.
46. Brill TB, Brush PJ, and Patil DG. Thermal decomposition of energetic materials 58. Chemistry of ammonium nitrate and ammonium dinitramide near the burning surface temperature. *Combust Flame* 1993; 92: 178–186.
47. Oxley JC, Smith JL, Rogers E, et al. Ammonium nitrate: thermal stability and explosivity modifiers. *Thermochim Acta* 2002; 384: 23–45.
48. Oxley JC, Smith JL, and Wang W. Compatibility of ammonium nitrate with monomolecular explosives. 2. Nitroarenes. *J Phys Chem* 1994; 98: 3901–3907.
49. Izato Y and Miyake A. Thermal decomposition of molten ammonium nitrate (AN). *J Therm Anal Calorim* 2015; 122: 595–600.

50. Andersen W, Bills K, Mishuck E, et al. A model describing combustion of solid composite propellants containing ammonium nitrate. *Combust Flame Combust Flame* 1959; 3: 301–317.
51. Brower KR, Oxley JC, and Tewari MP. Evidence for homolytic decomposition of ammonium nitrate at high temperature. *J Phys Chem* 1989; 93: 4029–4033.
52. Cagnina S, Rotureau P, Fayet G, et al. The ammonium nitrate and its mechanism of decomposition in the gas phase: a theoretical study and a DFT benchmark. *Phys Chem Chem Phys* 2013; 15: 10849–10858.
53. Cagnina S, Rotureau P, Fayet G, et al. Modeling chemical incompatibility: ammonium nitrate and sodium salt of dichloroisocyanuric acid as a case study. *Ind Eng Chem Res* 2014; 53: 13920–13927.
54. Sun J, Sun Z, Wang Q, et al. Catalytic effects of inorganic acids on the decomposition of ammonium nitrate. *J Hazard Mater* 2005; 127: 204–210.
55. Park J and Lin MC. Thermal decomposition of gaseous ammonium nitrate at low pressure: kinetic modeling of product formation and heterogeneous decomposition of nitric acid. *J Phys Chem A* 2009; 113: 13556–13561.
56. Shan T, van Duin ACT, and Thompson AP. Development of a reaxFF reactive force field for ammonium nitrate and application to shock compression and thermal decomposition. *J Phys Chem A* 2014; 118: 1469–1478.
57. Apostolescu N, Geiger B, Hizbullah K, et al. Selective catalytic reduction of nitrogen oxides by ammonia on iron oxide catalysts. *Appl Catal B Environ* 2006; 62: 104–114.
58. Vargeese AA and Muralidharan K. Kinetics and mechanism of hydrothermally prepared copper oxide nanorod catalyzed decomposition of ammonium nitrate. *Appl Catal A Gen* 2012; 447: 171–177.
59. Janssens W, Falsig H, Lundegaard LF, et al. A consistent reaction scheme for the selective catalytic reduction of nitrogen oxides with ammonia. *ACS Catal* 2015; 5: 2832–2845.
60. Chen H, Wei Z, Kollar M, et al. A comparative study of  $N_2O$  formation during the selective catalytic reduction of  $NO_x$  with  $NH_3$  on zeolite supported Cu catalysts. *J Catal* 2015; 329: 490–498.
61. Xu Z, Wang Q, and Fu X. Thermal stability and mechanism of decomposition of emulsion explosives in the presence of pyrite. *J Hazard Mater* 2015; 300: 702–710.